Journal of
Applied Remote Sensing

Ultra-compact imaging spectrometer for remote, *in situ*, and microscopic planetary mineralogy

Byron Van Gorp
Pantazis Mouroulis
Diana Blaney
Robert O. Green
Bethany L. Ehlmann
Jose I. Rodriguez

SPIE

Ultra-compact imaging spectrometer for remote, *in situ*, and microscopic planetary mineralogy

Byron Van Gorp,[a,*] Pantazis Mouroulis,[a] Diana Blaney,[a] Robert O. Green,[a] Bethany L. Ehlmann,[a,b] and Jose I. Rodriguez[a]

[a]Jet Propulsion Laboratory, California Institute of Technology, Pasadena, California 91109
[b]Division of Geological and Planetary Sciences, California Institute of Technology, Pasadena, California 91125

Abstract. The ultra-compact imaging spectrometer is a miniature imaging spectrometer that has been designed for compatibility with operation in a Martian environment. The spectrometer can be mated to a variety of front optics, both telescopic and microscopic. With a miniature telescope, it can serve as a rover mast instrument that surveys the surrounding area from a distance of ~1 m to infinity and produces full spectral data (500 to 2500 nm) of a wide panoramic scene in order to find the most mineralogically promising targets for further analysis and for directing subsequent rover activities. With a microscopic front lens, it can serve as an analytical tool for determining types of minerals in a rock and their spatial relations at a scale of tens of micrometers in order to make detailed interpretations of geological history. A realization of the instrument, adapted for operation in the Earth's atmosphere, has been produced and tested both in the laboratory and in the field. The results prove the ability of the instrument to detect and map minerals of interest in both modes of operation. © *2014 Society of Photo-Optical Instrumentation Engineers (SPIE)* [DOI: 10.1117/1.JRS.8.084988]

Keywords: imaging spectroscopy; imaging spectrometer; mineralogy; Mars rover; microspectroscopy.

Paper 14048SS received Jan. 22, 2014; revised manuscript received Mar. 20, 2014; accepted for publication Mar. 21, 2014; published online Apr. 25, 2014.

1 Introduction

Visible to short-wave infrared (VSWIR) spectroscopy is a powerful technique for identifying mineral types through absorption bands due to vibrations or electronic transitions. Detection of a wide range of minerals is possible and facilitated by the existence of spectral libraries.[1] Imaging spectroscopy adds a further dimension in mapping mineral location relative to a broader geologic context thus enhancing the understanding of geologic history. Mineral mapping through VSWIR spectroscopy has been demonstrated on Earth[2,3] and in other solar system bodies such as Mars[4–6] or the moon.[7,8] Future planetary exploration will also use this technique for remote mineralogy from orbit, fly-bys, and *in situ*.

VSWIR spectroscopy provides a means to tie together orbital and *in situ* observations with a single technique. Although the technique has been implemented mainly from orbiting or airborne remote sensing instruments, an *in situ* spectrometer could map minerals on spatial scales from meters to millimeters utilizing an appropriate front lens. However, to our knowledge, the technique has not been demonstrated in an imaging mode at the millimeters scale with an instrument adaptable to the demands of planetary missions. The MiniTES instrument[9] on the Mars Exploration Rovers is a thermal emission point spectrometer that requires a relatively long time to acquire the spectrum of a single point in the scene.

Reflectance spectroscopy provides useful data even at the microscopic level, thus spanning several orders of magnitude in spatial scale. In this sense, "remote" sensing can be extended to the microscale to provide nondestructive, noncontact information about individual rocks. There

*Address all correspondence to: Byron Van Gorp, E-mail: byron.e.van.gorp@jpl.nasa.gov

exists, however, an important difference between microscopy and *in situ* or remote sensing in that a microscope is generally required to carry its illumination source and the illumination conditions are critical. Reflectance spectroscopy of typical minerals at the microscopic level (60 to 100 μm) was demonstrated and the necessary illumination conditions established in Ref. 10. However, only a point spectrometer was used, and spectra were recovered at individual points or short linear traverses near boundaries. Full spectral image cubes were obtained with the Micromega instrument[11,12] by illuminating the sample with variable-wavelength monochromatic light. However, the technique cannot be extended to remote targets, where one must rely on ambient sunlight.

The ultra-compact imaging spectrometer (UCIS) is an imaging spectrometer system suitable for resource-constrained missions, where a compact instrument can be utilized for determining mineralogy of the surrounding terrain. Depending on the front optical system, it can serve in a remote, close-up, or microscopic implementation. The small volume of the instrument enables *in situ* observations using rovers and/or landers where the space and resources are highly constrained. The design seeks to advance the state-of-the-art in planetary spectrometers in terms of mass and volume savings without sacrificing the high uniformity and robustness of the present designs. Thus compared to the M^3 instrument, which to our knowledge is the lowest mass/highest uniformity instrument flown in space, we achieve a volume and mass reduction by a factor of $\sim$4 with no sacrifice in uniformity or instrument robustness.

Although we have labeled this instrument "ultra-compact," neither the spectrometer nor the telescope is the smallest design possible for these specifications. Rather than attempting to set a miniaturization record for the optomechanical bench, we decided to provide a design with space flight heritage, ease of assembly, and maximum stability. An all-aluminum reflective system is inherently athermal, quick to dissipate thermal transients, and is immune to radiation. Thus transmissive spectrometer designs such as the Dyson[13,14] or solid Offner[15] were excluded, even though they could provide some further miniaturization. Furthermore, we decided on a conventional Offner design with a combined primary/tertiary even though splitting this mirror in two separate ones can result in further mass savings.[16] The telescope is of a two-mirror design which is somewhat larger than alternative designs such as a three-mirror anastigmat for the same aperture and focal length. But as is the case with the spectrometer, the two-mirror system is very easy to assemble, and since the focal length is very small, the resulting mass or volume savings are small to negligible relative to the mass of the rest of the system.

2 UCIS for Remote or In Situ Sensing

When mated to a telescope front, UCIS can serve to obtain images and spectra at a distance from infinity to $\sim$1 m. Thus, it is suitable for an orbiter, a lander, or a rover, where, placed on a mast, it can survey the surrounding terrain for mineralogically interesting targets and guide further rover actions. We chose this implementation for an Earth surface demonstration instrument. It should be clear that the requirements for operation in the Earth's atmosphere and thermal environment lead to some different implementation choices compared with what would be appropriate for Mars. Only the core of the instrument that includes the optical bench, detector, and associated readout can be the same for both Earth and Mars. The thermal and data processing systems are different, though important features are retained and proven. The terrestrial version of UCIS operates in a vacuum instead of Mars atmospheric pressure, with the temperature excursions and ambient operating temperatures being significantly different. Also, the terrestrial data system is not limited by download speeds or memory, and we chose to take full advantage of that fact in order to examine the largest possible amount of data in the shortest time.

2.1 *Instrument Description*

UCIS comprises a miniaturized, all-reflective spectrometer of the Offner type,[13,17] and a small two-mirror telescope of 20-mm focal length. The spectrometer operates at $F/4$. Additional optical design details have been shown in Ref. 18. The focal plane detector array (FPA) is a Teledyne 6604A substrate-removed HgCdTe array with 640×480 pixels of 27 μm square size. The array

Table 1 Spectrometer characteristics.

Spectral	Range	500 to 2500 nm
	Sampling	10 nm
Spatial	Field of view	30 deg
	Instantaneous FOV	1.35 mrad
	Spatial swath	380 pixels
Radiometric	Range	0% to 100% R
	SNR	>300[a]
Uniformity	Spectral cross-track	>95%[b]
	Spectral instantaneous field of view mixing	<5%[c]

[a]See Fig. 9.
[b]Straightness and orientation of monochromatic slit image <5% of pixel width.
[c]Misregistration of spectrum to array row.

is not utilized in its entirety in either direction. An order-sorting filter with three segments is placed in close proximity to the detector surface. The basic system specifications are given in Table 1 and a photograph of the assembled system in Fig. 1. Uniformity errors have been described in Ref. 19.

Thermal components included in the vacuum enclosure are the cryo-cooler for controlling the FPA temperature and a thermo-electric Peltier cooler for controlling the spectrometer body temperature. The part of the system that is independent of operational environment (and thus would be the same for a planetary instrument implementation) is shown in Fig. 2. It includes the spectrometer and telescope, FPA and its mount, cold shield in front of array, thermal strap, and the cryocooler. Maintaining low mass for this subsystem is critical. For this reason, we show in Table 2 the mass breakdown arising from as-fabricated and assembled components.

The optical head and cryocooler have a combined mass of 643 g. The mass of the optical bench, including spectrometer, FPA assembly, and telescope is <340 g. The remaining 300 g is attributed to the thermal hardware. Relative to previous instruments such as M^3, additional significant mass reduction was found through the FPA mount design. The FPA assembly weighs <60 g compared to ~250g on the M^3 instrument.

The FPA is mounted to a six degrees of freedom mount allowing the stable mounting and fine adjustment to meet the instrument uniformity requirements. The FPA mount also provides thermal isolation from the spectrometer housing and an integral cold shield that are required in order to facilitate a higher operating temperature of 270 K for the spectrometer bench and telescope,

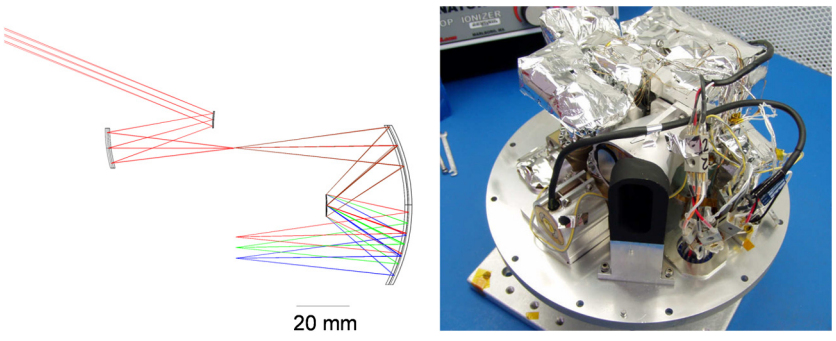

Fig. 1 Raytrace of ultra-compact imaging spectrometer (UCIS) spectrometer system and photograph with vacuum enclosure cover removed. The black painted part in the foreground is a baffle defining the telescope aperture. The diameter of the base plate is 20.3 cm. External to the vacuum enclosure are the thermal control and data processing electronics.

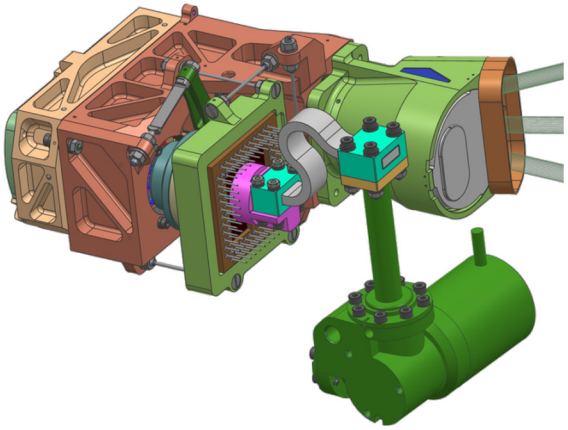

Fig. 2 UCIS instrument layout showing the Offner-type spectrometer, two-mirror telescope, FPA assembly, and cryo-cooler. This part of the instrument would be the same in a Mars rover or other space implementation.

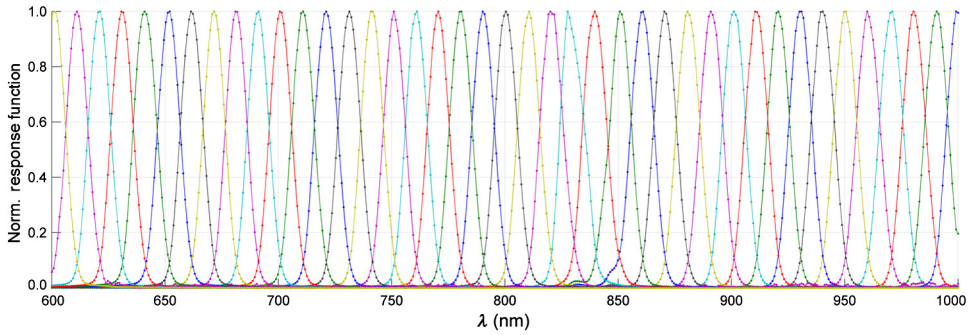

Fig. 3 Typical spectral response functions of UCIS. Shown here is the middle of the field of view and the range 600 to 1000 nm. All functions are normalized to unity at the peak. Raw data points (dark-subtracted detector readings) are plotted. Occasional glitches occur due to less than perfectly smooth monochromator scan. Each data point represents a pause in the scan and recording of the detector output.

Table 2 Optical head and cryocooler mass.

Description		Mass (g)
Thermal hardware	Ricor cryocooler	185
	Thermal strap	15
	Cryocooler hardware	65
	Spectrometer TEC/thermal strap	30
	Temperature sensors/adhesive	11
Optical bench	Spectrometer housing assm	124
	Spectrometer mirror assm	53
	Focal plane mount assembly	56
	Telescope assembly	72
	Fasteners	12
	Detector FPC	20
Optical head and cryocooler		643

which results in lower overall thermal loads in order to meet low power requirements as needed for *in situ* instruments on limited platforms. The FPA temperature set point is 170 K. The cold shield is maintained at ~230 K, while the spectrometer body is maintained at 273 K via a Peltier cooler.

2.2 *Laboratory Characterization*

The spectral and spatial responses of the system were measured in the laboratory for all wavelengths and several field points spanning the entire field of view of the telescope. A subset of results is shown below, beginning with representative spectral response functions shown in Fig. 3. These were taken using a scanning monochromator with a linewidth of <1 nm and recording the pixel response with increasing wavelength. For any given wavelength, through field full-width half maximum (FWHM) variation of <10% was demonstrated. The spectral response function FWHM is around 12 nm.

The spatial characteristics of UCIS were established through measurement of the cross-track and along-track spatial response functions (ARF and CRF) through field and wavelength. These are measured by scanning a subpixel slit placed at the focal plane of a collimator illuminating the instrument aperture, and oriented parallel (ARF) or perpendicular (CRF) to the spectrometer slit. Representative CRFs are shown in Fig. 4 for adjacent pixels and wavelengths spanning the spectral range. The FWHM is near 1.05 pixel units. The FWHM variation of the CRF with wavelength for each spatial field/focus position is <10%.

The CRF width variation with wavelength is an important aspect of uniformity and must be minimized. Figure 5 shows that it remains within 10% of a pixel throughout the wavelength range. The same figure also plots the CRF FWHM for three focus positions demonstrating the depth of focus of the instrument. Other locations in the instrument field of view give similar results.

The telescope response (ARF) was also measured through focus. Representative ARFs are shown in Fig. 6, showing a relatively small variation in width. Nominal telescope focus is set at ~4.5 m. A single wavelength is shown, but the response is essentially wavelength-independent.[20] In operation, these responses are convolved with scan smear.

A more direct visual representation of the close-up resolution of UCIS is given in Fig. 7, showing an image of a three-bar target at a distance of 1 m from the telescope. The just-resolved group has a bar size close to the angular sampling of UCIS. The curvature seen on the vertical edge is a telescope effect (the slit projection is not straight). This effect is routinely corrected in similar sensors to a high accuracy using a geometric camera model if desired.

A comparison was performed between UCIS and an analytical spectral devices (ASD) spectrometer commonly used as a field standard. In both cases, the raw spectrum of a doped

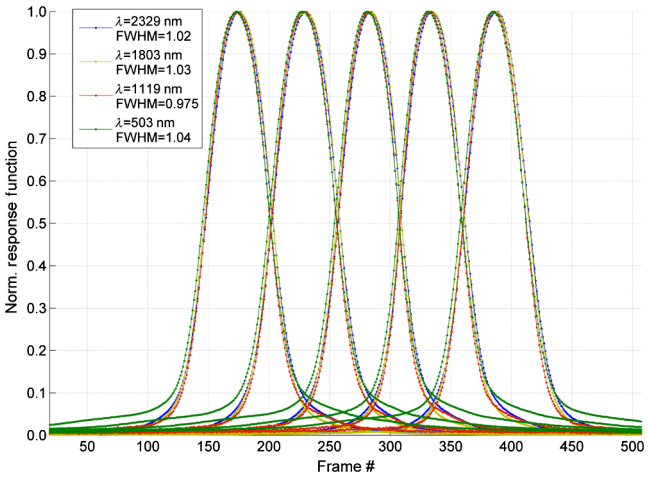

Fig. 4 Typical cross-track spatial response functions for adjacent pixels near the middle of the field of view and several wavelengths spanning the full range.

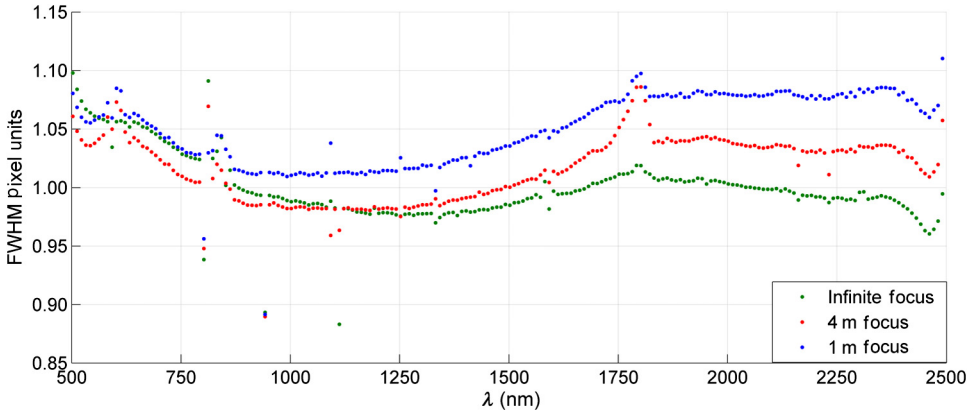

Fig. 5 CRF full-width half maximum variation throughout the spectral range for the middle of the field and three telescope focus positions.

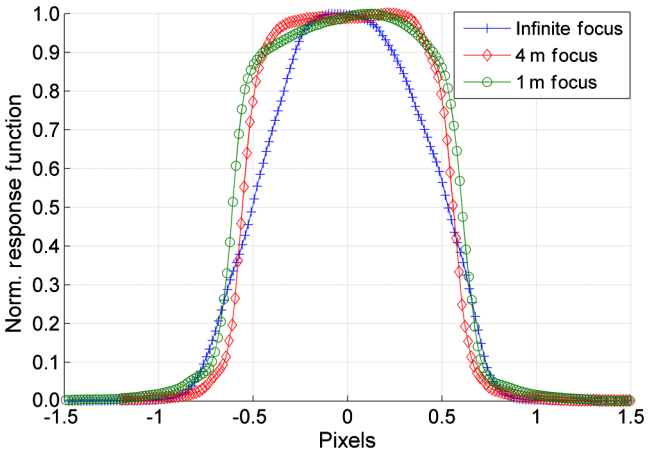

Fig. 6 Along-track response functions for several telescope focus positions and one wavelength.

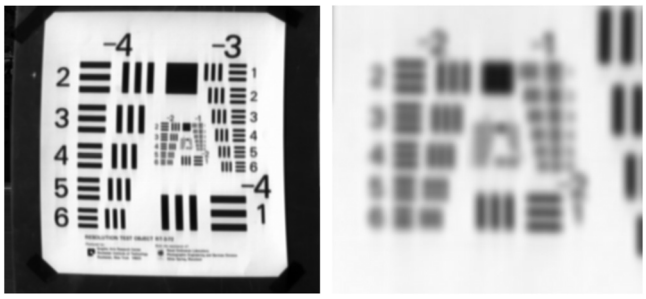

Fig. 7 Resolution target at 1-m distance, left, and zoom-in of the central portion. Bar size of the just-resolvable $(-2, 4)$ group is ~1.37 mm. A bad pixel effect is evident in the following group $(-2, 5)$.

spectralon panel was recorded and divided by the corresponding undoped panel. The result, shown in Fig. 8, demonstrates that UCIS operates well as a spectrometer with no obvious artifacts. The reduced modulation in the short wavelength features is thought to be due to a combination of stray light (inevitably greater in a pushbroom system relative to the ASD point spectrometer) and a short-wavelength detector response anomaly specific to the particular detector unit.

The instrument signal-to-noise ratio (SNR) is measured in the laboratory using an integrating sphere target and a tungsten halogen source. A filter combination provides a spectral radiance

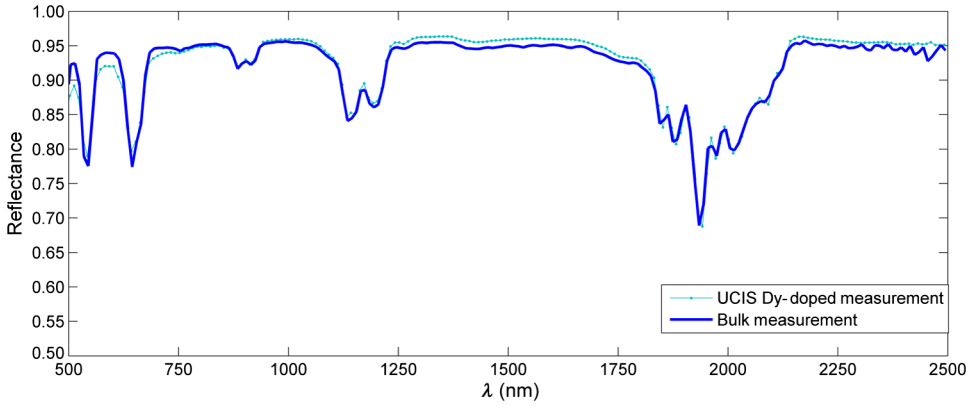

Fig. 8 Comparison between measured and reference dysprosium oxide-doped Spectralon panel spectra.

distribution that is closer (blue-shifted) to solar illumination than the raw lamp output. The radiance is measured with an independently calibrated spectrometer. Figure 9 shows the result for a single integration time of 15 ms. Although this result is obtained with a relatively bright target, typical conditions of operation permit averaging of several frames, thus compensating for potentially low target reflectance.

2.3 *Radiometric Calibration*

The radiometric calibration of UCIS differs from that of airborne or space sensors. To the extent that UCIS sees arbitrarily oriented surfaces in the natural environment and small areas of centimeters size or less, it cannot derive absolute target reflectance, lacking detailed knowledge of target illumination, and geometry at these scales. Rather, the aim of UCIS is to detect spectral signatures through diagnostic absorption bands. For this reason, in place of absolute radiometric coefficients for each spectral channel, UCIS relies on a relative comparison between the scene and a spectrally flat panel ("calibration target"). One such panel implementation is shown in Fig. 10. An attachment to the vacuum container was fabricated that can hold a 10-cm diameter Spectralon® panel. In imaging mode, the panel is removed and UCIS sees directly through the opening. In calibration mode, the panel is illuminated by the sun as shown in Fig. 10, with the diffusely reflected light at about 80 deg entering the telescope. The panel covers the entire field

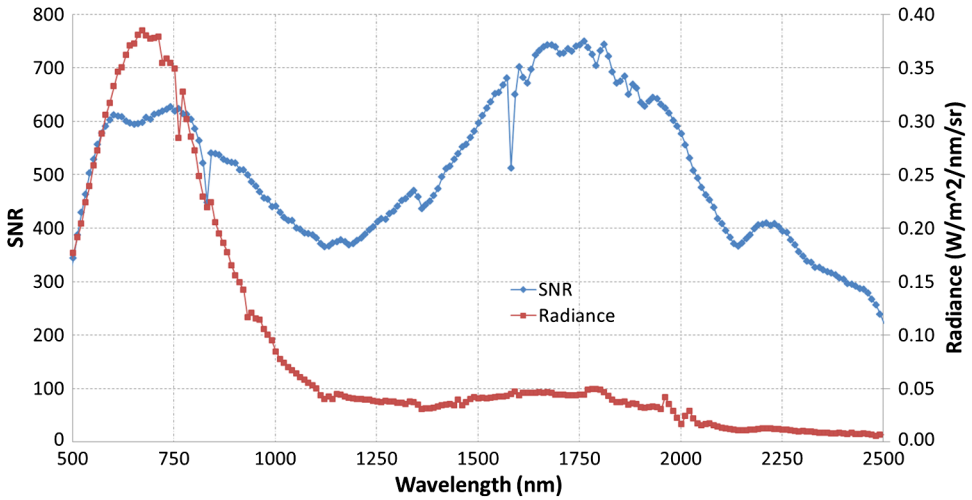

Fig. 9 UCIS signal-to-noise ratio (SNR) and corresponding reference radiance. The two SNR dips at ~830 and 1580 nm are due to the order-sorting filter seams which are nearly opaque.

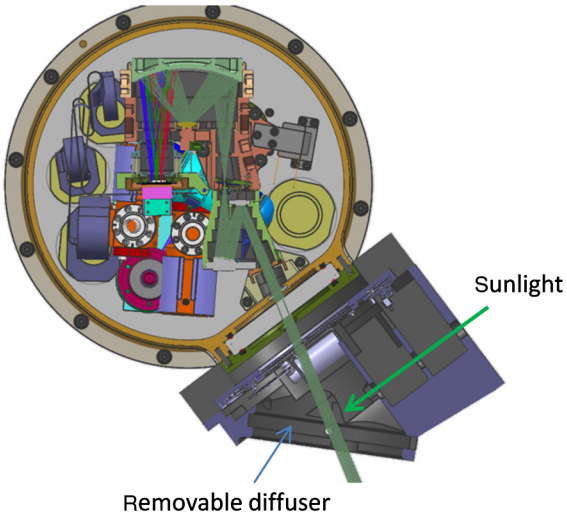

Fig. 10 Calibration target assembly. The removable diffuser allows direct view of the scene.

of view. Three baffles may be seen in front of the panel. Those limit the visible sky to a small slice, and therefore they also limit the amount of atmospherically scattered light reaching the panel. The result is a blue-poor illumination compared to a nonbaffled panel, or to the scene itself, i.e., preferential loss of atmospherically scattered light (Rayleigh, Mie) in favor of direct solar illumination. This effect is illustrated by comparing the spectrometer output using the arrangement of Fig. 10 against its output when viewing a large unobstructed Spectralon panel situated a few meters in front of the instrument that receives closer to full sky illumination. The ratio of the two measurements is shown in Fig. 11. It may be seen that the ratio drops at the short wavelength end following quadratic or higher power dependence. Although this ratio can be used as a correction factor, it should be evident that the field of view of any calibration target can never be exactly the same as that of the scanned target and some subtle spectral bias will always be present. However, the effect of such bias on mineral detection and identification based on distinct absorption features is minimal to negligible.

The strong irregularities in Fig. 11 occur near strong atmospheric absorptions where the signal and corresponding SNR is low. The peak near 1550 nm is a saturation/nonlinearity effect that was subsequently corrected with shorter integration time. The remaining smaller irregularities are due to instrumental drifts mostly due to the relatively high FPA operating temperature for these Earth surface measurements that will be mitigated in future upgrades to UCIS. The strong absorption of atmospheric water vapor near 1350, 1900, and 2500 nm regions and carbon dioxide near 2000 nm limit the utility of UCIS in the terrestrial atmosphere with its particular mix of gases for these spectral regions.

2.4 *Field Tests and Verification*

For field tests, the UCIS vacuum enclosure is situated on a rotation stage and a tripod, together with the FPA and thermal control electronics (Fig. 12). Housekeeping electronics and a processing computer are carried in a small portable rack. The rotation stage and the recording are controlled by an additional laptop computer. UCIS has been tested in the Jet Propulsion Laboratory (JPL) Mars Yard as well as at sites around Mono Lake in California. We present below a small subset of results to confirm the ability of the instrument to detect and identify minerals of interest.

Figure 13 shows an RGB scaled image from UCIS of a 90 deg scan of the JPL Mars Yard, taken at a rate of ~28 deg / min. Several interesting mineralogical samples and other test targets are located throughout the field to demonstrate the spectral capability, ability to map minerals, and the effects of range on measurement. A smaller section of this image is analyzed in Figs. 14 and 15. Individual spectra from the sample rocks of Fig. 13 were extracted and compared to laboratory spectra in Fig. 14. There is a good agreement with the spectral shape and band

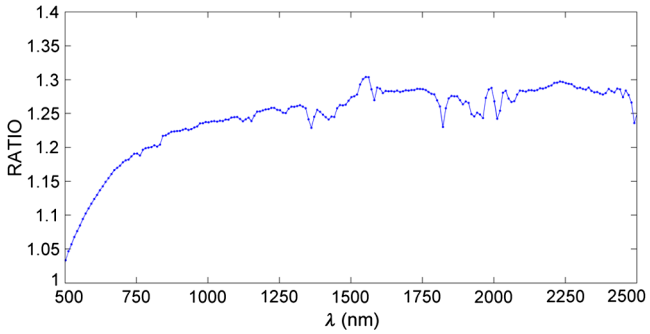

Fig. 11 Comparison between baffled calibration target and large spectralon panel in front of the instrument that sees additional sky irradiance.

position. Variations in absolute reflectance are expected since no detailed corrections have been made for solar illumination and observation geometry. This, however, does not impact the ability to discriminate between these minerals. Gaps in the Mars Yard spectra are due to the complete attenuation of sunlight by water in the Earth's atmosphere. On Mars, with its much drier atmosphere, these gaps would not be present in the spectra.

Figure 15 shows the ability to map mineral throughout the scene. For olivine, carbonate, and gypsum, the data were processed to produce mineral distribution maps based on the bands shown in Fig. 14 using the parameterization developed for compact reconnaissance imaging spectrometer for Mars (CRISM).[21] In Fig. 15, a color composite of the image is shown simulating what the eye sees: most of the rocks and soils look either red or white. However, the mineral parameter maps demonstrate how key minerals stand out against their surroundings even when they are localized to small areas. Range to target has little impact on the results as shown by comparing the spectra for gypsum sand at 7, 15, and 20 m. This is not unexpected since the atmospheric

Fig. 12 UCIS optical head assembly, rotation stage/tripod. Since the photo was taken, a computer-controlled external shutter was added for collecting dark frames automatically.

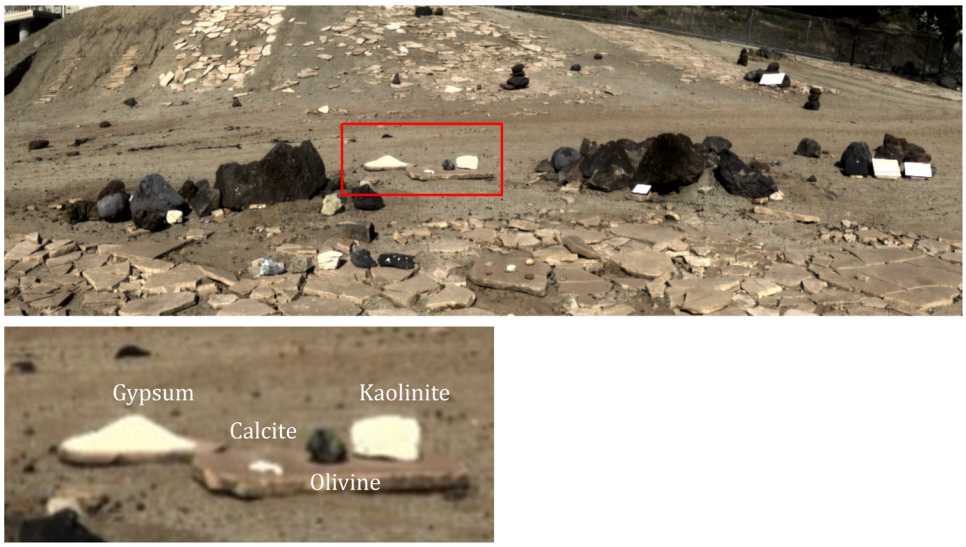

Fig. 13 RGB image of JPL Mars Yard scan and enlargement of central region where the spectra were extracted for comparison with laboratory spectra.

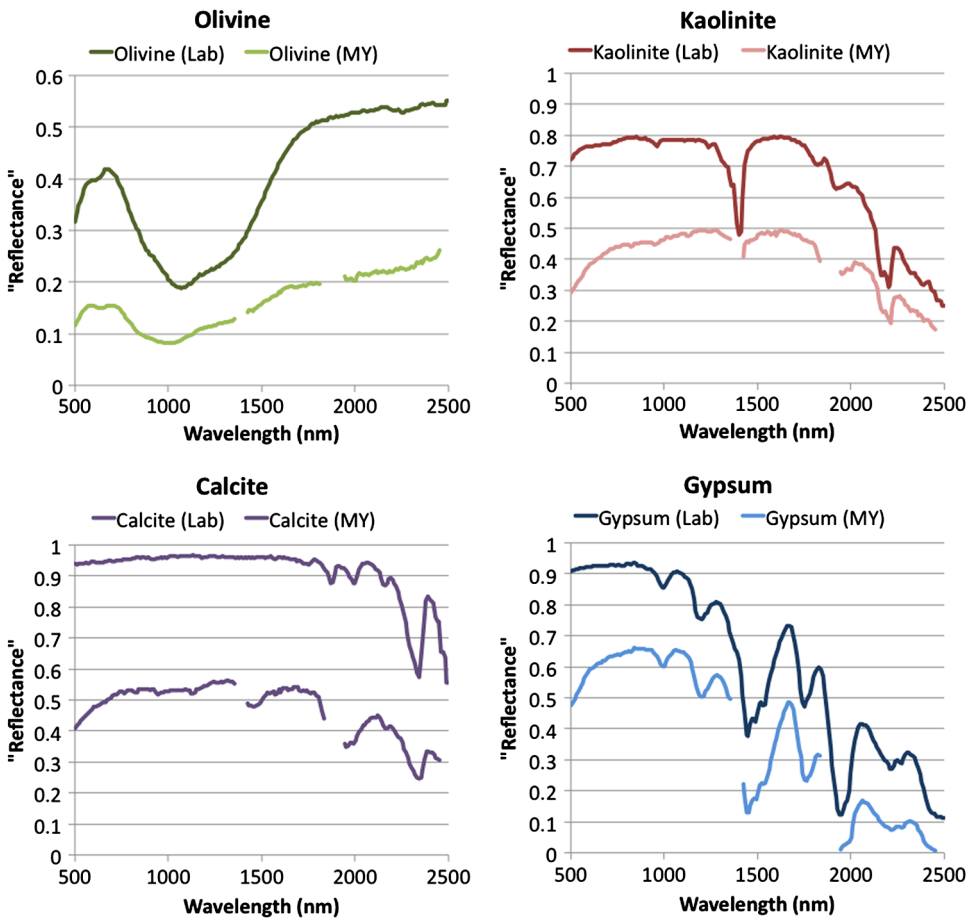

Fig. 14 Extracted spectra for gypsum, calcite, olivine, and kaolinite compared to laboratory spectra of the same minerals from the USGS spectral library (Ref. 1).

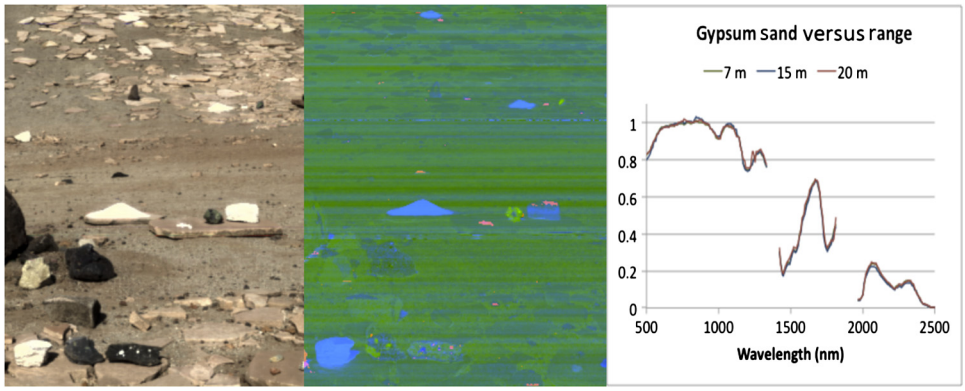

Fig. 15 (a) RGB image of scanned region. (b) False color composite of gypsum band depth map (blue), olivine index (green), and carbonate depth map (red). (c) Single spectra extracted from image cube, normalized to unity at 822 nm, from gypsum sand placed at 7, 15, and 20 m away from the instrument.

effects on the solar spectrum are dominated by the top-of-atmosphere to surface path making the effects of range to target a minor perturbation to the spectrum.

3 UCIS as Microspectrometer

3.1 *Microspectroscopy Setup and Characteristics*

Since UCIS was already packaged with its telescope in a vacuum enclosure, which is necessary for operation in the Earth's atmosphere, the best solution for using it in a microscopic mode was to construct an optical adapter that transforms the telescope into a microscope and can be attached externally to the vacuum shell. This was achieved with a system of two spherical mirrors and three flat fold mirrors. The combined effect of the UCIS telescope and adapter is to provide a ~3× magnification of the detector pixel/slit at the sample location. The pixel footprint at the sample is ~81 μm. The beam F-number is multiplied by the same factor, so the object-space beam is $F/12$, thus providing a ~2-mm depth of field. The combination of UCIS with this microscope front end is designated micro-UCIS.

In operation, the sample to be scanned is mounted on a translatable holder that provides scan and focus. For planetary and space applications, it would be desirable to transfer the scan movement to the instrument rather than the sample, and Fig. 16 shows a design that achieves this with a single fold mirror that can be rotated for the scan and translated for focus.

In the laboratory setup for micro-UCIS, illumination comes from two linear fiber bundles with special fibers that have no absorption features within the UCIS spectral range. These bundles are fed by a single quartz-halogen lamp, coupled to the input using uncoated CaF_2 optics. In an eventual rover instrument, the fiber bundles would be substituted with independent lamps. The use of two independent lamps is useful for reducing shading on a rough sample and generally reducing artifacts arising from illumination directionality such as localized specular reflections. It also provides some redundancy should one lamp fail. Our lamp and fiber setup was not optimized for efficiency, and only a small fraction of the 100 W lamp output ends up on the sample. For Mars or other planetary missions where the power constraints may be significant, this inefficiency is not normally acceptable. Modeling and additional laboratory experiments show that a sufficiently bright and uniform field can be obtained with two 5 W tungsten lamps placed inside appropriately designed reflectors.

The spectral characteristics of UCIS remain unchanged. Its spatial characteristics retain the near-Gaussian form of the response function. An example CRF is shown in Fig. 17 for several wavelengths, confirming the high uniformity of the instrument. The depth of focus is assessed by fitting Gaussians to the through-focus response and plotting the standard deviation (Sigma) as a function of distance (Fig. 18). Sigma stays within 15% of minimum over a focus distance of 2 mm.

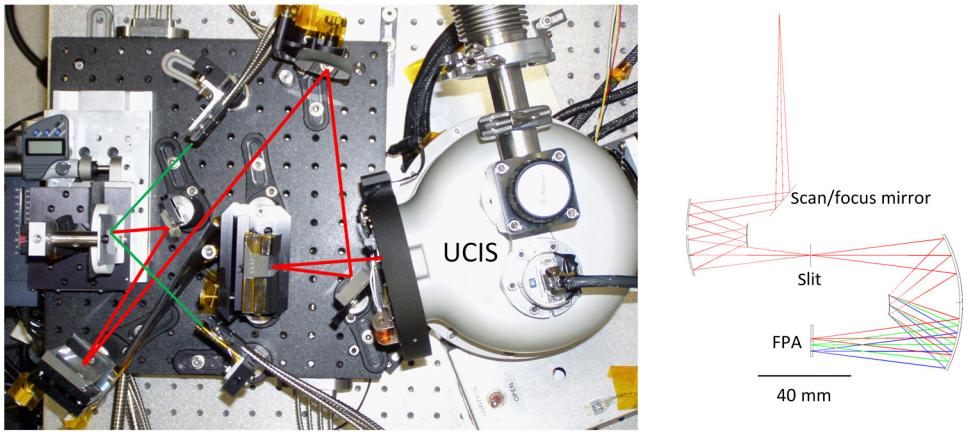

Fig. 16 UCIS in microscope mode. Light from the sample follows the red path to the telescope. The direction of illumination is shown by the two green lines. Also shown is a raytrace of a microscope relay for replacing the combined UCIS telescope and laboratory microscopic adapter that achieves the same specifications as the laboratory breadboard.

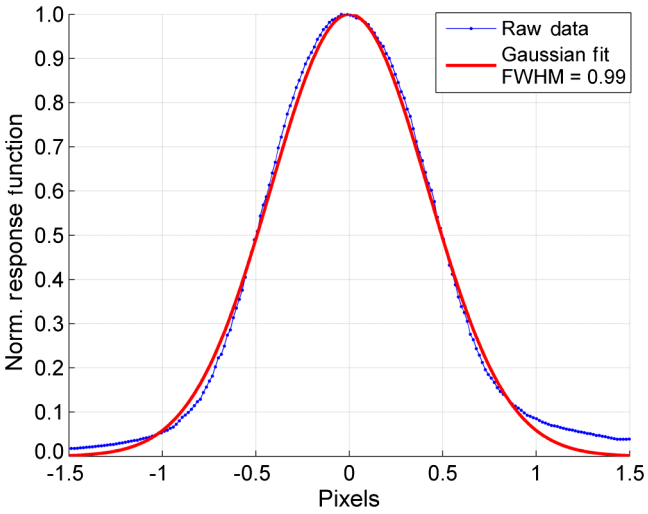

Fig. 17 UCIS CRF in microscope mode for several pixels at a wavelength of 2269.5 nm. Raw data and a Gaussian fit function are shown.

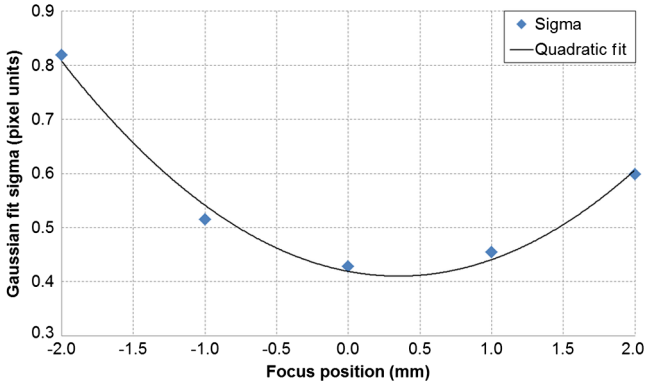

Fig. 18 UCIS depth of focus in microscope mode. Points show response width Sigma at specific focus positions. A fitted quadratic curve is also shown.

3.2 *Rock Spectral Analysis Examples*

In laboratory operation, the spectrum of a sample is obtained by dividing the dark-subtracted sample data by dark-subtracted spectralon data, with a measurement taken of a spectralon panel at the location of the rock sample. For a space instrument where the panel cannot be placed, calibration is done using a combination of monitoring lamp output and subtracting the actively illuminated scene from the passively illuminated scene, coupled with occasional flat field and calibration verification checks by measurement of the inside of an instrument cover. Typical integration time is 20 ms and typical frame averaging is 14 frames. Thus a square (380×380) image is acquired in ~108 s. However, this acquisition time reflects a limitation of the maximum speed of the translation stage we used. The system supports a much faster rate, by a factor of 3 or more, while still maintaining SNR above 100. Thus UCIS can have a significant acquisition time advantage over Micromega with its stated 500 s acquisition time per image cube for a SNR of >100. UCIS also collects a 380 square image as opposed to a 256 square image for Micromega.[12] The comparison has some validity despite the different areas and resolutions imaged by the two instruments because UCIS illumination would increase if the area was to decrease to the smaller Micromega footprint, thus maintaining SNR. The UCIS acquisition can be slowed down to offer improved SNR for measurements of special importance or exceptionally low albedo targets.

Figure 19 illustrates the acquisition of data over a rather dark (visible albedo <0.1 polished slab from a banded iron formation. Electronic transitions due to hematite can be easily discerned at 530 and 860 nm. Distinguishing hematite with different microcrystalline absorptions is possible via study of broadband absorption properties. The vibrational absorption of chert (hydrated silica) is visible near 2200 nm. Additional sharp vibrational absorptions due to organics allow their detection. Using techniques identical to those employed by orbiting imaging spectrometers,[21] mapping these in band depth strength maps across the sample permits mapping mineral distribution. Although a few pixels (<10%) cannot be used in detailed analysis due to specular reflection or instrument effects (bad detector pixels), most pixels provide single pixel detection capability for key mineral and organic species. Figure 20 demonstrates this single pixel utility with a roughly cut sandstone surface. In this sample from a stromatolite, distinctive sand-sized mineral grains have unique vibrational absorption features characteristic of particular carbonates and clay minerals. A band of sedimentary rock with calcium carbonate is distinguished by a

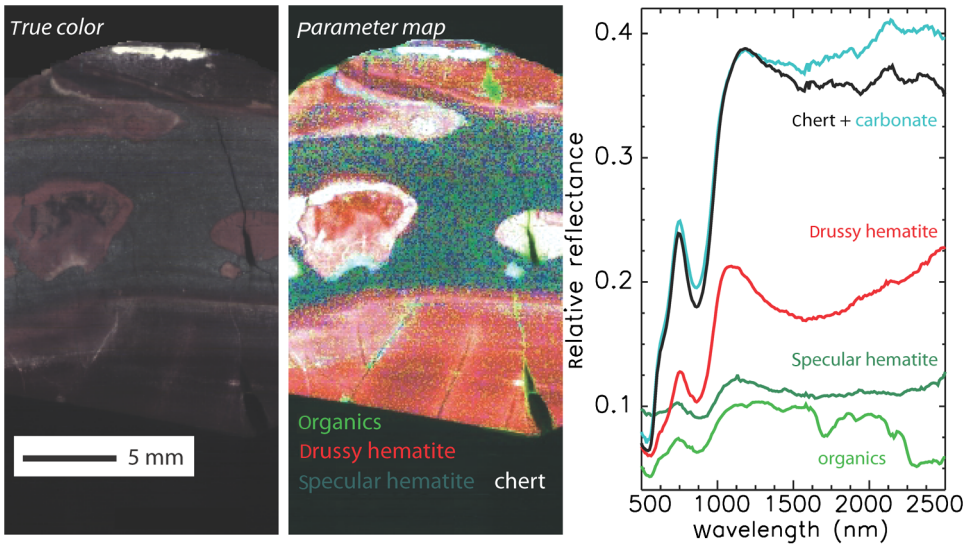

Fig. 19 (a) A visible color microimage of a rock sample from a banded iron formation. (b) A parameter map (red; 860-nm band depth, green: 1750-nm band depth, and blue: 2210-nm band depth) allows mapping discrete spectral characteristics and mineral phases. (c) Single pixel or 3×3 spectra from UCIS reveal Fe(III) oxides and chert. Even organics from a resin used in sample preparation can be mapped.

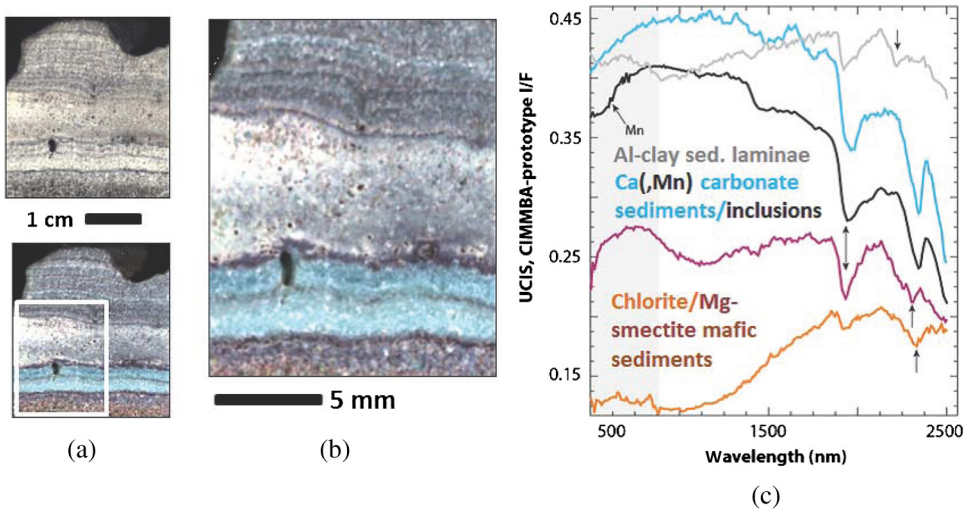

Fig. 20 (a) The UCIS footprint of a stromatolite in visible wavelengths (top) and shortwave infrared wavelengths (bottom; R: 2400 nm, G: 1800 nm, and B: 960 nm), highlighting how key aspects of mineralogic variability are apparent only by looking at longer wavelengths. (b) A zoom of the lower left showing the resolution of single grains within the sandstone (c) single pixel spectra from location in the sandstone show distinctive sources of sediments that formed the rock and two generations of carbonate in a distinctive blue band with dark vugs filled with minerals. Above the carbonate are aluminum-rich clay minerals and below it are magnesium-rich chlorites and smectites.

2340-nm absorption, and filled dark vugs have carbonate with iron and manganese, which generates an electronic transition absorption at shorter wavelengths. The laminated sediments above the carbonate have Al-clay minerals, identified by 1900-nm H_2O and 2210-nm Al-OH absorptions, while those below have coarser grains which vary between Mg-OH absorptions indicating smectite clays (2320 nm) or chlorite (2330 nm). Such high resolution data of mineralogic variability are of high utility for petrographic study, i.e., the joint study of mineralogy with texture. For example, Fig. 20 shows the changing of the sedimentary source materials from mafic (magnesium-, iron-rich rocks) to felsic (aluminum-, silica-rich), separated by an interval of carbonate formation. UCIS's fine scale resolution of mineralogy permits these distinctive processes and their timing to be discerned, a capability not possible with bulk measurement over the entire sample footprint.

4 Conclusions

A compact, rover-compatible imaging spectrometer operating in the solar reflected spectral range has been developed and demonstrated. UCIS is suitable for a wide range of planetary surface mineralogy and compositional mapping objectives accommodating spatial scales from meters to millimeters. In UCIS, this capability is achieved with an optical head mass of <0.4 kg that includes the spectrometer, telescope, detector, and mount. A complete field system was assembled, and was shown to acquire high quality spectra of a 90 deg × 30 deg panorama (1160 × 380 pixels) in just over 3 min. A companion microspectroscopy capability has been demonstrated with UCIS and used to collect micro-UCIS data sets at the 80 μm sampling scale. With this microspectroscopy capability, an additional set of fine scale mineralogy objectives may be achieved. For both implementations, UCIS has been shown to meet the key spectrometer specifications desired for an *in situ* instrument, including spectral/spatial uniformity throughout the telescope focus range of 1 m to infinity.

An optical adapter allows conversion of UCIS for operation at microscopic spatial scales with a pixel footprint of 81 μm and a depth of field of ~2 mm. Spectra of ~30 mm square areas were acquired at minute-scale time intervals with halogen lamp illumination. The resulting spectra demonstrated the use of the instrument for performing the rock sample petrography at microscopic spatial scales.

UCIS and micro-UCIS demonstrate a path to extend orbital VSWIR imaging spectroscopy to the rover scale from ~1 m to the horizon, as well as the microscopic scale for detailed petrologic investigations. VSWIR imaging spectroscopy provides an important means to tie together orbital and *in situ* observations with a single analytical technique.

Acknowledgments

This research has been performed at the Jet Propulsion Laboratory, California Institute of Technology, under a contract with the National Aeronautics and Space Administration. The authors thank the UCIS project team members Daniel W. Wilson, Brandon Richardson, R. Glenn Sellar, Howard Tseng, Michael Eastwood, Hal Sobel, Mark Helmlinger, Morgan Cable of JPL, and Christopher Edwards (Caltech) for their contribution to this work. Reference herein to any specific commercial product, process, or service by trade name, trademark, manufacturer, or otherwise, does not constitute or imply its endorsement by the United States Government or the Jet Propulsion Laboratory, California Institute of Technology. The authors thanks the J. Grotzinger and W. Fischer for providing geologic samples.

References

1. R. N. Clark et al., USGS Digital Spectral Library splib05a, U.S. Geological Survey, Open File Report 03–395, http://pubs.usgs.gov/of/2003/ofr-03-395/datatable.html (2003).
2. R. N. Clark et al., "Imaging spectroscopy: Earth and planetary remote sensing with the USGS Tetracorder and expert systems," *J. Geophys. Res.* **108**(E12), 5131–5175 (2003), http://dx.doi.org/10.1029/2002JE001847.
3. R. O. Green et al., "Imaging spectroscopy and the airborne visible/infrared imaging spectrometer (AVIRIS)," *Rem. Sens. Environ.* **65**(3), 227–248 (1998), http://dx.doi.org/10.1016/S0034-4257(98)00064-9.
4. J. P. Bibring et al., "Mars surface diversity as revealed by the OMEGA/Mars express observations," *Science* **307**(5715), 1576–1581 (2005), http://dx.doi.org/10.1126/science.1108806.
5. S. Murchie et al., "Compact reconnaissance imaging spectrometer for Mars (CRISM) on Mars reconnaissance orbiter (MRO)," *J. Geophys. Res. Planets* **112**(E5), E05S03 (2007), http://dx.doi.org/10.1029/2006JE002682.
6. S. L. Murchie et al., "A synthesis of Martian aqueous mineralogy after one Mars year of observations from the Mars Reconnaissance Orbiter," *J. Geophys. Res. Planets* **114**(E2), E00D06 (2009), http://dx.doi.org/10.1029/2009JE003342.
7. C. M. Pieters et al., "Character and spatial distribution of OH/H_2O on the surface of the Moon seen by M3 on Chandrayaan-1," *Science* **326**(5952), 568–572 (2009), http://dx.doi.org/10.1126/science.1178658.
8. P. J. Isaacson et al., "Remote compositional analysis of lunar olivine-rich lithologies with Moon Mineralogy Mapper (M-3) spectra," *J. Geophys. Res. Planets* **116**(E6), E00G11 (2011), http://dx.doi.org/10.1029/2010JE003731.
9. P. R. Christensen et al., "Miniature thermal emission spectrometer for the Mars Exploration Rovers," *J. Geophys. Res. Planets* **108**(E12), 8064 (2003), http://dx.doi.org/10.1029/2003JE002117.
10. P. Mouroulis et al., "Reflectance microspectroscopy of natural rock samples in the visible and near infrared," *Appl. Spectrosc.* **62**(12), 1370–1377 (2008), http://dx.doi.org/10.1366/000370208786822160.
11. V. Leroi, J.-P. Bibring, and M. Berthe, "Micromega/IR: design and status of a near-infrared spectral microscope for *in situ* analysis of Mars samples," *Planet. Space Sci.* **57**(8–9), 1068–1075 (2009), http://dx.doi.org/10.1016/j.pss.2008.12.014.
12. C. Pilorget and J.-P. Bibring, "NIR reflectance hyperspectral microscopy for planetary science: application to the MicrOmega instrument," *Planet. Space Sci.* **76**, 42–52 (2013), http://dx.doi.org/10.1016/j.pss.2012.11.004.
13. L. Mertz, "Concentric spectrographs," *Appl. Opt.* **16**(12), 3122–3124 (1977), http://dx.doi.org/10.1364/AO.16.003122.

14. P. Mouroulis et al., "A compact, fast, wide-field imaging spectrometer system," *Proc. SPIE* **8032**, 80320U (2011), http://dx.doi.org/10.1117/12.882706.
15. C. P. Warren et al., "Miniaturized visible near-infrared hyperspectral imager for remote-sensing applications," *Opt. Eng.* **51**(11), 111720 (2012), http://dx.doi.org/10.1117/1.OE.51.11.111720.
16. P. Mouroulis, "Low-distortion imaging spectrometer designs utilizing convex gratings," *Proc. SPIE* **3482**, 594–601 (1998), http://dx.doi.org/10.1117/12.322062.
17. D. Kwo, G. Lawrence, and M. Chrisp, "Design of a grating spectrometer from a 1 : 1 Offner mirror system," *Proc. SPIE* **818**, 275–279 (1987), http://dx.doi.org/10.1117/12.978898.
18. B. Van Gorp et al., "Optical design and performance of the ultra-compact imaging spectrometer," *Proc. SPIE* **8158**, 81580L (2011), http://dx.doi.org/10.1117/12.892422.
19. P. Mouroulis, R. O. Green, and T. G. Chrien, "Design of pushbroom imaging spectrometers for optimum recovery of spectroscopic and spatial information," *Appl. Opt.* **39**(13), 2210–2220, http://dx.doi.org/10.1364/AO.39.002210.
20. B. Van Gorp et al., "Ultra-compact imaging spectrometer (UCIS) for in-situ planetary mineralogy: laboratory and field calibration," *Proc. SPIE* **8515**, 85150G (2012), http://dx.doi.org/10.1117/12.939475.
21. S. M. Pelkey et al., "CRISM multispectral summary products: parameterizing mineral diversity on Mars from reflectance," *J. Geophys. Res. Planets* **112**(E8), E08S14 (2007), http://dx.doi.org/10.1029/2006JE002831.

Biographies of the authors are not available.